Journal of the Optical Society of Korea
Vol. 20, No. 2, April 2016, pp. 245-250

ISSN: 1226-4776(Print) / ISSN: 2093-6885(Online)
DOI: http://dx.doi.org/10.3807/JOSK.2016.20.2.245

Single Exposure Imaging of Talbot Carpets and Resolution Characterization of Detectors for Micro- and Nano- Patterns

Hyun-su Kim[1,2]*, Serhiy Danylyuk[3], William S. Brocklesby[2], and Larissa Juschkin[1]

[1]*Chair for the Experimental Physics of Extreme Ultraviolet, RWTH Aachen University and JARA-FIT, Steinbachstrasse, 15, 52074 Aachen, Germany*
[2]*Optoelectronics Research Center, University of Southampton, Southampton, SO17 1BJ, UK*
[3]*Chair for the Technology of Optical Systems, RWTH Aachen University, and JARA-FIT, Steinbachstrasse, 15, 52074, Aachen, Germany*

(Received December 30, 2015 : revised February 25, 2016 : accepted February 29, 2016)

In this paper, we demonstrate a self-imaging technique that can visualize longitudinal interference patterns behind periodically-structured objects, which is often referred to as Talbot carpet. Talbot carpet is of great interest due to ever-decreasing scale of interference features. We demonstrate experimentally that Talbot carpets can be imaged in a single exposure configuration revealing a broad spectrum of multi-scale features. We have performed rigorous diffraction simulations for showing that Talbot carpet print can produce ever-decreasing structures down to limits set by mask feature sizes. This demonstrates that large-scale pattern masks may be used for direct printing of features with substantially smaller scales. This approach is also useful for characterization of image sensors and recording media.

Keywords : Talbot effect, Self-imaging, Micro-imaging, Nano-structuring, Extreme ultraviolet
OCIS codes : (110.2970) Image detection systems; (110.6760) Talbot and self-imaging effects; (350.5500) Propagation; (120.3940) Metrology; (260.7200) Ultraviolet, extreme

I. INTRODUCTION

In this paper, we present a submicron patterning method for optical Talbot carpet in a single exposure configuration. We also demonstrate a rigorous simulation for Talbot carpet in nano-scale. In principle, the Talbot carpet originally has an analogy in quantum physics referred to as the "quantum carpet", which describes the behaviour of localized wave packets, which undergo revivals in time [1]. The Talbot carpets are also found in atomic physics [2], in plasmonics [3, 4], and especially in wave propagation in coherent optics.

Talbot carpet of light is a longitudinal section (in direction of propagation) of the interference pattern behind a 1-dimensional transmission grating illuminated by a coherent plane wave. An image of Talbot carpet contains fractional profiles of a master grating at rational multiples of the Talbot distance. It also contains profiles of fractal Talbot patterns at irrational fractions of the Talbot distance [5-7]. Accordingly, Talbot carpet is highly interesting since the scaling down of feature size is among the critical issues and challenges for submicron to nano-patterning [8, 9].

Talbot images or near-field interference patterns behind periodic grating structures were first observed by H. Talbot, who discovered that, at regular distances behind the plane structure, a pattern that replicates the original grating structure is formed [10]. L. Rayleigh explained that the replication distance, z_T, of this optical pattern under illumination with a monochromatic plane wave is determined by the period of the object structure (d) and by the wavelength (λ) of the incident light, and he derived a relation for the distance, known since then as the "Talbot length", $\{z_T=2d^2/\lambda\}$ [11]. The phenomenon can be explained by Fresnel diffraction theory of the periodic object [12-14]. The repeating patterns are not only seen at positive integer multiples of the Talbot length, $n \cdot z_T$, but also at fractional intervals, $\{(p/q) \cdot z_T/2\}$, where p and q are coprime positive integer numbers [5, 15, 16].

*Corresponding author: hk1u12@soton.ac.uk

Color versions of one or more of the figures in this paper are available online.

While fractional Talbot patterns are cross-sections of intensity distribution orthogonal to the light propagation axis, patterns at the plane containing the optical axis are referred to as a "Talbot carpet" or "carpet of light" [6].

In our interest, the visualization of the optical Talbot carpet is usually performed by computer integration of images recorded by digital camera at different distances from the grating [17-20]. However, in order to obtain the image of the Talbot carpet, a large number of such high-resolution images are required.

Previously, the measurements were done in the visible spectral range and with a large period grating, which made the measurement simpler. Particularly, in the case of submicron gratings, the spatial resolution of optical detectors is not sufficient, so the good way to image the pattern is to record each plane by exposure of photo-sensitive materials such as photoresists [21]. However this is a tedious and time-consuming procedure requiring repeated nano-meter precise positioning of the photoresist plane. Therefore we consider a single exposure imaging method that can record the high-resolution structure of Talbot carpets over a wide range of propagation distances without missing image planes, which can also become a fundamental technique to investigate and utilize the nano Talbot carpets.

In simulation, we study further for a non-paraxial case of Talbot pattern employing finite-difference time-domain (FDTD) simulation by the "Dr Litho" simulator [22, 23]. In this demonstration, extreme ultraviolet (EUV) radiation is used, which can be realized lithographically [24]. We analyse for image properties especially in the rational and irrational intensity profiles in the Talbot carpet. The simulation results show the single exposure configuration for Talbot carpet can produce the ever-decreasing periodicities in nano-scale down to diffraction limit in intensity profiles.

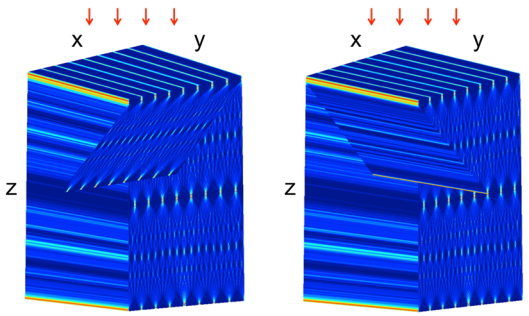

(a) (b)

FIG. 1. Talbot pattern behind a grating in space under coherent plane illumination from top: Traditional Talbot carpet is seen in x-z plane. The two diagonal cross-sections display (a) Talbot carpet, and (b) a pattern consisting of various pitches.

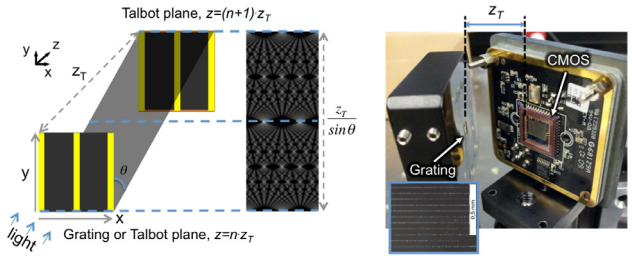

(a) (b)

FIG. 2. (a) The geometrical concept of the single exposure imaging of Talbot carpet, (b) Experimental setup showing the alignment between the grating and the detector: the inset image shows the microscope image of the grating.

II. ANALYSIS OF TALBOT CARPET

2.1. Images of Talbot Carpet

It is well known that the Talbot pattern is a Fresnel image that can be calculated by the angular spectrum representation within Fourier optics [25]. This solution is valid under paraxial approximation when $d^2/z > \lambda$. The intensity distribution behind a grating is shown in Fig. 1. The initial intensity distribution is considered as a binary transmittance, $u(x, z=0) = 1$ within the opening and $u = 0$ within the absorber line (slit width = 0.1 × period), where x is the coordinate perpendicular to the grating rulings and z is the axis of the illuminating light-wave propagation. The object is assumed as an ideal binary periodic grating that is infinitely repeated along the x- and y- axes. The Talbot pattern is formed behind this object through the space.

In considering the diagonal cross-sections through the 3-dimensional (3D) image of the Talbot pattern, such a cross-section as shown in Fig. 1(a) shows the Talbot carpet stretched in the z-direction in comparison to the conventional Talbot carpet formed just in the x-z plane. This diagonal cross-section contains the complete Talbot carpet, because all details of the intensity distribution at each z-position are included in those tilted 2D images (diagonal cross-section in Fig. 1(a)). In the space of the Talbot pattern, another diagonal cross-section in Fig. 1(b) is the line-and-space image rather than the traditional Talbot carpet image, which consists of gradually smaller (or bigger) pitches between neighbours.

2.2. Single Exposure Imaging of Talbot Carpet

The method uses a fact that the Talbot carpet is actually located over x-, y-, z-axes, while the conventional method is to scan the profile in the x-axis through the propagation axis as mentioned (see the axis definition in Fig. 2(a)). Here we use diagonal cross-sections in the 3D Talbot pattern to obtain a full image of the Talbot carpet. The object in this case is an ideal binary line-space grating, which is infinitely repeated with a certain period. The object has no variation along the y-axis, and so for the interference image behind the grating, no intensity change exists along the y-axis, while the intensity is modified along the x-axis.

Thus, in the x-y plane at any Talbot distances ($z = n \cdot z_T$,

n is positive integer), a cross-section at $y = y'$ (any value) is identical. A diagonal plane placed with one side at a Talbot plane ($z = n \cdot z_T$) and with its other side at the following the Talbot plane ($z = (n+1) \cdot z_T$) with any different y-position as shown in Fig. 2(a) contains full information about the Talbot pattern. Therefore, a Talbot carpet can be constructed from the image recorded by a planar detector such as a digital camera or photoresist coated wafers positioned diagonally in the single exposure configuration.

III. RESULTS

3.1. Experimental Demonstration: Imaging of the Talbot Carpet

In this section, we demonstrate imaging of Talbot carpets in experiments. The exposure was performed with plane wave illumination generated by a highly coherent *HeNe* laser (λ = 632.8 nm). The incident beam has illuminated a transmission mask that is a laser-milled steel grating consisting of 60 μm pitch and 10 μm slit width. The grating field size in the mask was 10 mm × 10 mm. A high-resolution complementary metal-oxide-semiconductor (*CMOS*) image sensor was used to detect the image. The resolution of the image sensor is 1280 × 1024 pixels in 6.6 mm × 5.3 mm area. Fig. 2(b) displays the experimental setup showing configuration of the grating mask and the detector. The detector plane was aligned diagonally as in Fig. 1(a) with an angle of around θ = 45°.

Figure 3(a) shows the result that the Talbot carpet is obtained by the single exposure configuration. The image is recorded in z range between $z=z_T$ and $z=2 \cdot z_T$, which corresponds to a full Talbot period. The intensity change in center in Fig. 3(a) occurred due to repositioning of the detector that covers a half of the z_T (~1 mm).

The resulting image is stretched in propagation direction due to the tilt in comparison to the traditional Talbot carpet formed in the x-z plane. The stretched length (Talbot period) in the tilted plane is magnified by $1/\sin\theta$, where θ is an angle of the detector plane from the grating plane. Thus the period of the Talbot carpet (z_T) becomes $\{z_T/\sin\theta\}$ in the detector. Intensity profiles of the Talbot carpet between experiment and simulation are plotted in Fig. 3(c) and (d) respectively. The periods of particular patterns exhibit integer multiples of period of master object at $\{z=(1/M)(z_T/2)\}$, where *M* is a positive integer, which corresponds to spatial frequency multiplication.

This method allows characterizing the capability of detectors particularly in terms of resolution. In this demonstration, we used a conventional *CMOS* imaging sensor, which consists of ~ 5.2 μm period between photodiodes. However as can be seen in Fig. 3(c), the detector can distinguish the intensity profile up to M=3, while simulation performs up to M=4. It implies that the resolution of the detector is around 20 μm. In principle, at least three pixels are required to detect a pitch, which corresponds to 15.6 μm, but

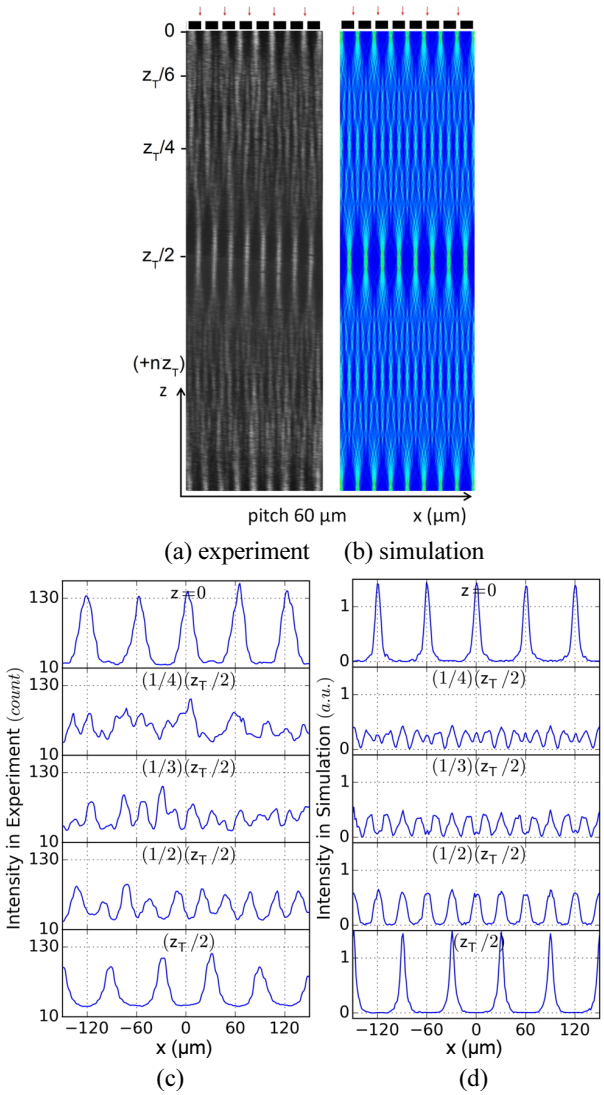

FIG. 3. (a) The experimental image of Talbot carpet, (b) the simulated image of Talbot carpet and the intensity profiles of (c) experimental and (d) simulated data at several fractions of the Talbot distance.

imperfect grating features affect the image contrast. Thus, resolution can be smaller than 20 μm, but not smaller than 15 μm as in theory. The visibilities for intensity profiles in the experiment are compared with the one in simulation where visibility is defined as: $\{V=(I_{MAX} - I_{MIN})/(I_{MAX} + I_{MIN})\}$. Visibility in the experiment (V_1) is decreased in comparison with visibility in the simulation (V_0) over fractional Talbot patterns. Thus, detection error (%): $\{(1-V_1/V_0)\times100\}$ is increased as M is increased as shown in Fig. 4. The error is nearly 40% at 30 μm period pattern.

While the Talbot carpet is visualized with a detector positioned perpendicular to the rulings and tilted in the y-z plane as shown in Fig. 1(a) for a horizontal grating, on the other hand, another pattern can be observed with a detector positioned parallel to the rulings and tilted in the x-z plane as shown in Fig. 1(b) for a vertical grating [26].

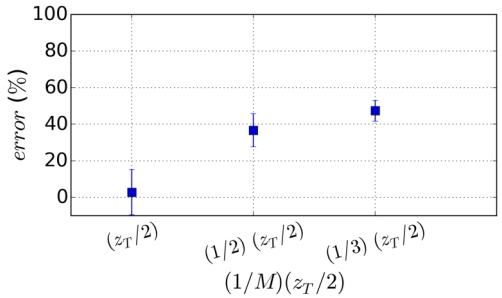

FIG. 4. Visibility errors by detector for fractional Talbot patterns.

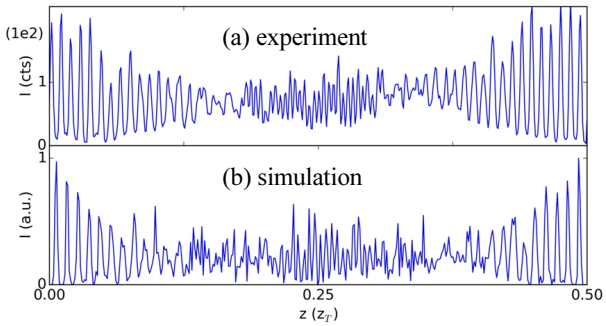

FIG. 5. Intensity profiles along the groove in the diagonal cross-section in Fig. 1(b) in experiment (top) and in simulation (bottom).

Such a result obtained in our experiment is presented in Fig. 5(a). The cross-sectional curves (1D profile) of the tilted image (2D image such as a diagonal section in Fig. 1(b)) are displayed in Fig. 5(a) in the range of a half Talbot distance. This profile exhibits various gaps between the peaks through the groove. The gradually increased or decreased gap through the groove is seen in a line-art profile as shown in Fig. 5 for simulation (top) and experiment (bottom), while the profiles of the fractional Talbot pattern show a regular gap as shown in Fig. 3(c, d). The gap (peak to peak) is magnified by $(1/\sin\theta)$ in comparison with the spatial frequency in fractional Talbot intensity profiles due to the broadening by tilt.

3.2. Talbot Carpet in Nano-scale: FDTD Simulation

In this section, we demonstrate FDTD simulations with EUV radiation at 13.5 nm wavelength in order to observe the smallest feature in the Talbot carpet. By employing FDTD simulation we can predict the smallest feature in Talbot carpet that will form in the area close to the grating, where the Fresnel-Kirchhoff assumption is not valid. In this regime, the multiple-slits interference influence is reduced but the single slit diffraction features becoming more important. With slit width approaching the wavelength of light the system is entering a non-paraxial regime requiring rigorous calculation. The optical properties of the Talbot image, particularly the intensity, the contrast and the interference

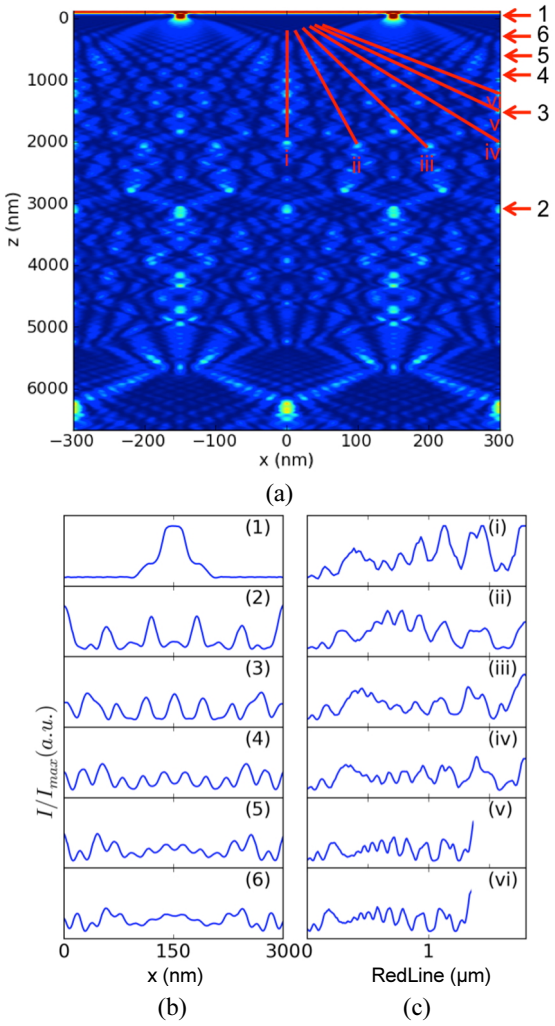

FIG. 6. (a) Talbot carpet calculated by FDTD simulation: (b) and (c) are intensity profiles along various detecting planes.

fringe quality are dependent on the geometry of the mask and the choice of materials. The large contrast between the transmission of the opening and of the absorber is required and the transmittance has to be optimized with the efficient thickness of the layers for both substrate and absorber in order to obtain the sharper image of the Talbot carpet. For example, in the model we demonstrate for the mask, the pitch was 300 nm, the opening-width was 20 nm and the line-width was 280 nm. The gold is deposited as an absorber layer (60 nm) on Si_3N_4 membrane (20 nm). This feature is realistic in current mask fabrication technology for EUV radiation [27]. X-ray data for optical properties of materials in [28] were used in the simulation.

Figure 6(a) displays the simulated image of the Talbot carpet behind the grating in the range of $z = 0$ to $z_T/2$ (0 - 6670 nm). The Talbot carpet in nano-scale is obtained in this case. Figure 6(b) and 6 (c) are intensity profiles that are determined at positions marked with red arrows (1)-(6) and red lines (i)-(vi) in Fig. 6(a). In both cases, intensity profiles reproduce self-images progressively at smaller scales

from 300 nm to 10 nm pitches depending on the detector plane such as planes at normal to z-axis (1-6) or tilted planes (i-vi).

For the case of fractional Talbot pattern as shown Fig. 6(b), spatial frequency is multiplied by up to a factor 15, which results in a corresponding half pitch of 10 nm. The visibility was from 2% at worst and 26% at best. In Fig. 6(c), the fractal Talbot intensity is shown at irrational cross-section as described by Berry [6, 29]. In this case, the width of peaks is decreased along the curves until no peak appears. The contrast is also decreasing as the width decreases and it finally becomes zero at some point, which corresponds to the diffraction limit.

IV. DISCUSSION

In comparison to conventional methods, the single exposure imaging method enables fast imaging of Talbot carpets, and also depth of focus becomes less critical, because no differential positioning of the detector is required. The experiment can be performed despite the imperfect quality of the grating due to the fact that the Talbot effect reproduces the self-image with modified quality from the grating [30, 31]. This is a well-known effect. However, this is an advantage when applying the method with gratings of smaller pitch.

The single exposure imaging method could be applied for rapid characterization of sources in metrology, where the wave propagation image over near- and far- fields is used for the analysis [20]. The method also enables printing Talbot carpets on photoresist samples using an interference lithography technique. Nano-scale Talbot carpet and fractal Talbot patterning may be feasible utilizing this method.

The rigorous diffraction simulation model has shown that the nano-scale Talbot carpet can be obtained under a coherent extreme ultraviolet radiation. Sub-10 nm scale structures may be realized in this case, while the conventional methods can hardly achieve that. The Talbot effect is valid within the limitation that no evanescent fields are present, and so spatial resolution is limited by diffraction. Thus, a highly efficient diffraction mask and a good coherent illumination exposing large area are required. The standard sample suggested in the FDTD simulation is a good example in this case.

We also suggest that structuring of Talbot carpets can be used for characterization of photoresist. While conventional deep ultraviolet optical lithography meets the demand to continuously shrink device structures, further steps of structure miniaturization can be obtained by EUV lithography [32]. The resolvability of photoresist becomes important in sub-10 nm lithography [21]. Thus this work may be potentially useful for applications of nano-lithography with highly coherent EUV sources [33]. Other possible applications would be nano-structuring of quantum dot arrays, nano-photonic devices, and nano-crystals [34-36].

V. CONCLUSION

We present an imaging technique that can perform visualization of Talbot carpets very simply and also precisely. Talbot carpet includes fractional and fractal patterns that feature ever decreasing periodicities in intensity profiles even though a large-scale period in mask is used. The experiment demonstrates that Talbot carpet as a whole can be reproduced in a single exposure configuration. The conventional Talbot carpet and another cross-sectional pattern are visualised with tilted detectors, where the tilting is in the range for detectable angle. It is shown that the method can be applied for resolution characterization of detectors. The method enables characterizing the resolvability of photoresist with high-resolution Talbot image produced by short wavelength radiation. Talbot carpet in nano-scale can be produced with the method introduced here, while conventional methods can hardly achieve this. We utilize FDTD simulations in order to observe the smallest feature of Talbot carpet in non-paraxial condition. Structures down to 10 nm are achieved using a 300 nm pitch mask and 13.5 nm wavelength illumination. It may be feasible structuring of Talbot carpet in nano-scale lithographically as suggested. The method could be potentially useful for characterization of light sources, nano-structuring, or applications in photonic devices.

ACKNOWLEDGMENT

This work is associated with the EU FP7 Erasmus Mundus Joint Doctorate Programme EXTATIC under framework partnership agreement FPA-2012-0033. L.J. acknowledges financial support by the Helmholtz Association for a Helmholtz Professorship as a part of the Pact for Research and Innovation. Authors would like to thank Dr. K. Bergmann and Prof. Dr. P. Loosen from Fraunhofer Institute for Laser Technology in Aachen, Germany for their great supports.

REFERENCES

1. O. Friesch, W. Schleich, and I. Marzoli, "Quantum carpets woven by Wigner functions," New J. Phys. **2**, 4 (2000).
2. M. Chapman, "Near-field imaging of atom diffraction gratings the atomic Talbot effect," Phys. Rev. A **51**, R14 (1995).
3. M. R. Dennis, N. I. Zheludev, and F. J. G. Abajo, "The plasmon Talbot effect," Opt. Express **15**, 9692-9700 (2007).
4. S. Cherukulappurath, D. Heinis, J. Cesario, N. F. Hulst, S. Enoch, and R. Quidant, "Local observation of plasmon focussing in Talbot carpets," Opt. Express **17**, 23772-23784 (2009).
5. M. V. Berry and S. Klein, "Integer, fractional and fractal Talbot effects," J. Mod. Opt. **43**, 2139-2164 (1996).
6. M. Berry, I. Marzoli, and W. Schleich, "Quantum carpets, carpets of light," Physics World **June**, 1-6 (2001).
7. M. Segev, M. Soljačić, and J. M. Dudley, "Fractal optics and beyond," Nature Photonics **6**, 209-210 (2012).

8. G. E. Moore, "Cramming more components onto integrated circuits," Electronics Magazine **38**, 114-117 (1965).
9. The International Technology Roadmap for Semiconductors, http://www.itrs.net (2013).
10. H. F. Talbot, "Facts relating to optical science No. IV," Philos. Mag. **9**, Series 3, 401-407 (1836).
11. L. Rayleigh, "XXV. On diffraction-gratings, and on some phenomena connected therewith," Philos. Mag. **11**, Series 5, 196-205 (1881).
12. J. M. Cowley and A. F. Moodie, "Fourier images I - The point source," Proc. Phys. Soc. B **70**, 486-496 (1957).
13. W. D. Montgomery, "Self-imaging objects of infinite aperture," J. Opt. Soc. Am. **57**, 772-775 (1967).
14. R. F. Edgar, "The Fresnel diffraction images of periodic structures," Opt. Acta **16**, 281-287 (1969).
15. P. Latimer and R. F. Crouse, "Talbot effect reinterpreted," Appl. Opt. **31**, 80-89 (1992).
16. H. C. Rosu, J. P. Trevino, H. Cabrera, and J. S. Murguia, "Self-image effects in diffraction and dispersion," Electromagnetic Phenomena **6**, 216-223 (2006).
17. S. Nowak, Ch. Kurtsiefer, T. Pfau, and C. David, "High-order Talbot fringes for atomic matter waves," Opt. Lett. **22**, 1430-1432 (1997).
18. W. B. Case, M. Tomandl, S. Deachapunya, and M. Arndt, "Realization of optical carpets in the Talbot and Talbot-Lau configurations," Opt. Express **17**, 20966-20974 (2009).
19. N. Guerineau, E. D. Mambro, and J. Primot, "Talbot experiment re-examined: study of the chromatic regime and application to spectrometry," Opt. Express **11**, 3310-3319 (2003).
20. N. Guerineau, B. Harchaoui, and J. Primot, "Talbot experiment re-examined: demonstration of an achromatic and continuous self-imaging regime," Opt. Commun. **180**, 199-203 (2000).
21. N. Mojarad, J. Gobrecht, and Y. Ekinci, "Beyond EUV lithography: a comparative study of efficient photoresists performance," Scientific Reports **5**, 1-7 (2015).
22. A. Erdmann, P. Evanschitzky, G. Citarella, T. Fühner, and P. De Bisschop, "Rigorous mask modeling using waveguide and FDTD methods: An assessment for typical hyper na imaging problems andreas," Proc. SPIE **6283**, 628319-1~628319-11 (2006).
23. S. Danylyuk, P. Loosen, K. Bergmann, H.-S. Kim, and L. Juschkin, "Scalability limits of Talbot lithography with plasma-based extreme ultraviolet sources," J. Micro/Nanolith. MEMS MOEMS **12**, 033002-1~033002-7 (2013).
24. H. H. Solak and Y. Ekinci, "Achromatic spatial frequency multiplication: A method for production of nanometer-scale periodic structures," J. Vac. Sci. Technol. B **23**, 2705-2710 (2005).
25. J. W. Goodman, *Introduction to Fourier Optics*, 2nd ed. (McGraw Hill, New York, USA, 1996).
26. J. A. Thomas, "Binaere phasenelemente in photoresist," Diploma Thesis, Friedrich-Alexander-Universität Erlangen-Nürnberg, Germany (1988).
27. S. Brose, S. Danylyuk, L. Juschkin, C. Dittberner, K. Bergmann, J. Moers, G. Panaitov, St. Trellenkamp, P. Loosen, and D. Grützmacher, "Broadband transmission masks, gratings and filters for extreme ultraviolet and soft X-ray lithography," Thin Solid Films **520**, 5080-5085 (2012).
28. X-ray Database, http://henke.lbl.gov/optical_constants
29. B. Mandelbrot, "How long is the coast of Britain? Statistical self-similarity and fractional dimension," Science **156**, 636-638 (1967).
30. K. Patorski, "The self-imaging phenomenon and its applications," in *Progress in Optics XXVII*, E. Wolf, ed. (Elsevier Science Publishers, Warsaw, Poland, 1989), pp. 2-108.
31. J. Wen, Y. Zhang, and M. Xiao, "The Talbot effect: recent advances in classical optics, nonlinear optics, and quantum optics," Advances in Optics and Photonics **5**, 83-130 (2013).
32. C. Wagner and N. Harned, "EUV lithography: Lithography gets extreme," Nature Photonics **4**, 24-26 (2010).
33. J. S. Chun, S.-H. Jen, K. Petrillo, C. Montgomery, D. Ashworth, M. Neisser, T. Saito, L. Huli, and D. Hetzer, "SEMATECH's cycles of learning test for EUV photoresist and its applications for process improvement," Proc. SPIE **9048**, 90481Z (2014).
34. E. Ozbay, "Plasmonics: Merging photonics and electronics at nanoscale dimensions," Science **311**, 189-193 (2006).
35. T. F. Krauss, R. M. De La Rue, and S. Brand, "Two-dimensional photonic-bandgap structures operating at near-infrared wavelengths," Nature **383**, 699-702 (1996).
36. M. Reed, J. Randall, R. Aggarwal, R. Matyi, T. Moore, and A. Wetsel, "Observation of discrete electronic states in a zero-dimensional semiconductor nanostructure," Phys. Rev. Lett. **60**, 535-537 (1988).